II. THE INFLUENCE OF Ag+Mg ADDITIONS CN THE

NUCLEATION OF STRENGTHENING PRECIPITATES

IN A NON-COLD-WORKED Al-Cu-Li ALLOY

THE INFLUENCE OF Ag+Mg ADDITIONS ON THE NUCLEATION OF STRENGTHENING PRECIPITATES IN A NON-COLD-WORKED Al-Cu-Li ALLOY

Introduction

Aluminum-copper-lithium alloys generally require cold work to attain their highest strengths in artificially aged tempers (1,2). These alloys are usually strengthened by a combination of the metastable $\delta'(Al_3Li)$ and $\theta'(Al_2Cu)$ phases and the equilibrium T_1 (Al_2CuLi) phase (3), where the T_1 phase is a more potent strengthener than the δ' (4). Various investigators, such as Cassada et al. (5) and Lee and Frazier (6), have shown that the high strengths obtained after artificial aging associated with cold work result from the heterogeneous precipitation of T_1 on matrix dislocations.

Pickens and coworkers (7-9) have shown that the Al-(4-6.3)Cu-1.3Li-0.4Ag-0.4Mg-0.14Zr (wt%) alloy Weldalite™ 049 attains ultra-high strengths in artificially aged tempers both with and without prior cold work (i.e., the T8 and T6 tempers, respectively). The T8 temper is primarily strengthened by a uniform distribution of fine T_1-type[*] platelike precipitates with a {111} habit plane (8), whose nucleation is stimulated by the Ag+Mg additions (7,8). These precipitates are also observed in the T6 temper. Moreover, Gayle et al. (10,11) identified numerous strengthening phases in non-cold-worked, artificially aged conditions, with the T_1 phase being predominant at peak strength. The resulting ultra-high strength in the T6 temper (i.e., without cold work) gives Weldalite™ 049 many potential advantages over other

---

[*] The strengthening phase is referred to as T_1-type because of difficulties in unambiguously indexing it as the T_1-phase or Ω-phase due to the similarities in the electron diffraction patterns from the two phases (8).

Al-Cu-Li alloys. The objective of the work reported here is to elucidate the mechanism by which the Ag+Mg additions stimulate the precipitation of T_1-type precipitates without cold work. To accomplish this, the microstructure of an Al-6.3Cu-1.3Li-0.14Zr model alloy was evaluated in a T6-type temper with and without the Ag+Mg addition.

Materials and Experimental Procedure

Two billets weighing 23 kg each were cast at Martin Marietta Laboratories and extruded into 0.95 x 10.2-cm bars at a ratio of 20:1 at International Light Metals, Torrance, CA. After extrusion, the bars were solution-heat-treated (SHT) at 504°C and water-quenched to ambient temperature. Compositions were measured from the extruded bar using the inductively coupled plasma technique (Table 1).

TABLE 1

Alloy Compositions

		Cu	Li	Zr	Ag	Mg	Al
049 [0Ag+0Mg]	nominal wt%	6.30	1.30	0.14	--	--	bal
	measured wt%	5.83	1.25	0.14	0	0	bal
	at%	2.48	4.85	0.04	--	--	bal
049	nominal wt%	6.30	1.30	0.14	0.40	0.40	bal
	measured wt%	6.47	1.25	0.14	0.40	0.40	bal
	at%	2.77	4.88	0.04	0.10	0.43	bal

The alloys will be referred to as 049 and 049 [0Ag+0Mg] as shown. Specimens were artificially aged and examined by transmission electron microscopy (TEM) with a JEOL 100CX. TEM foils were prepared with a Struers Tenupol using an electrolyte of one part HNO_3 in three parts methanol.

Results

Both alloys were evaluated by TEM after aging for 24 h at 180°C. This temper was chosen based on the tensile strength aging curve for alloy 049. The ultimate tensile strength (UTS), yield strength (YS), and percent elongation (%el) for the alloys in this temper were: 675 MPa YS, 707 MPa UTS, and 3.7% el for alloy 049, and 345 MPa YS, 478 MPa UTS, and 8.3% el for alloy 049 [0Ag+0Mg].

The selected-area electron diffraction pattern (SADP) for 049[0Ag+0Mg] with B = [100] (Fig. 1a) shows streaking in the <100> directions, with more intense streaks in one direction than the other. The <100> streaking is also present on the SADP with B = [110] (Fig. 1b). These <100> streaks result from θ' precipitates (12) and have maximum at the aluminum spots and at the superlattice positions. No other streaking or reflections is present on SADPs for either zone axis.

Faint but continuous streaking in the <111> direction is present on the SADP from 049 [0Ag+0Mg] with B = [112] (Fig. 1c). Two sets of reflections are present, one at 1/2 {220}, 1/3 {220}, and 2/3 {220}, and another at 1/3 and 2/3 {042}. Satellite (at arrow in Fig. 1c) spots along the <042> direction appear to be related to these reflections. Similar <111> streaking and

049 [0Ag + 0Mg] T6

B=[100]   B=[110]   B=[112]
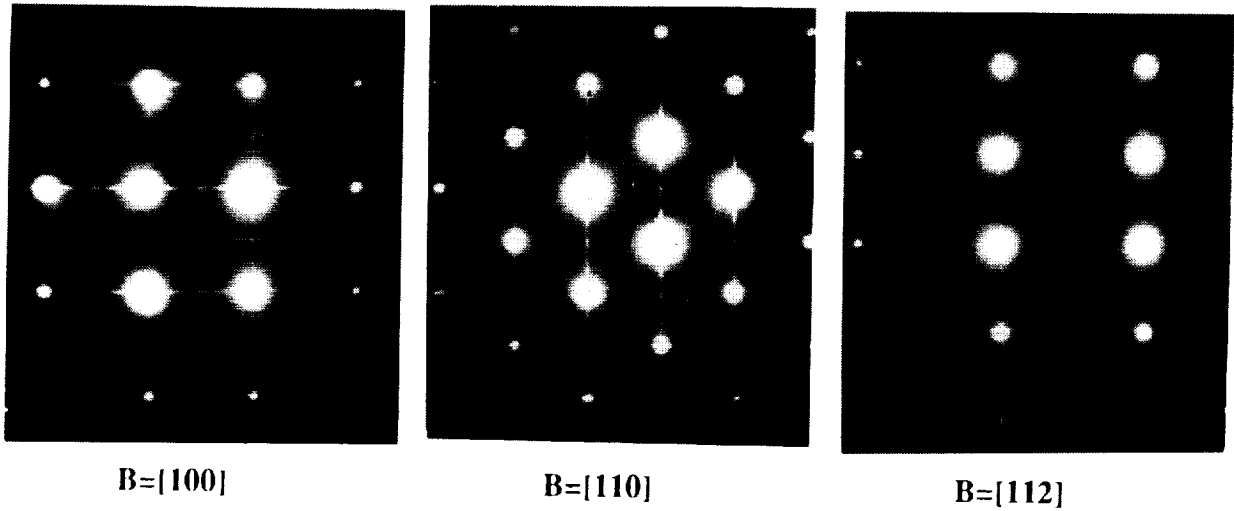
FIG. 1   SADPs for alloy 049 [0Ag+0Mg] T6 with (a) B = [100],
        (b) B = [110], and (c) B = [112].

reflections at 1/3 and 2/3 {220} were indexed as the T_1 phase in alloy 2090 by Huang and Ardell (4).

The SADP for 049 with B = [100] (Fig. 2a) shows reflections centered at 1/3 {220} and 2/3 {220}, which result from the intersection of two streaks in reciprocal space. Thus, when the deviation parameter ($\bar{s}$) is equal to zero, these reflections are single spots. When $\bar{s}$ does not equal zero, two satellite spots are present, separated by a distance that varies with $\bar{s}$. Similar reflections at 1/3 {220} and 2/3 {220} are also present on the SADP with B = [110] (Fig. 2b), accompanied by streaks in the <111> directions with diffuse maxima at approximately 1/2 {111}. No <100> streaking is present on the SADPs with B = [110] or [100]. Sharp <111> streaking with maxima at 1/4, 1/2, and 3/4 {111} is also present on the SADP with B = [112] (Fig. 2c). Elongated reflections are present at 1/3 {131}, 2/3 {131}, 1/3 {042}, and 2/3 {042}. These reflections, and the <111> streaking, result from T_1-type precipitates on {111} planes. The superlattice reflections at 1/2 {220} probably result from Al_3Zr.

A brightfield (BF) micrograph of 049[0Ag+0Mg] (Fig. 3a) shows θ' precipitates surrounding heterogeneous T_1 platelets. The brightfield was imaged with B = [110] so that one set of θ' precipitates is oriented normal to the plane of the foil and, thus, is viewed nearly edge on. The darkfield (DF) micrograph, which was imaged using the superlattice maxima on the <100> streak, shows a θ' precipitate-free zone (PFZ) surrounding the T_1 platelets (Fig. 3b). A θ' PFZ is also present next to the grain boundary (GB) in the upper right-hand corner of the micrograph.
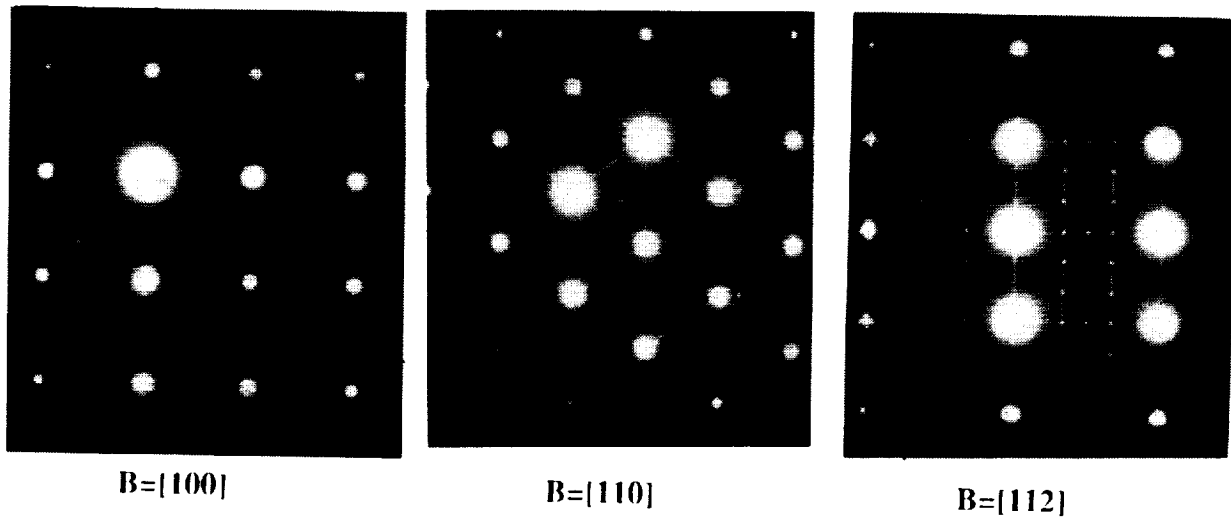
049 T6

B=[100]   B=[110]   B=[112]

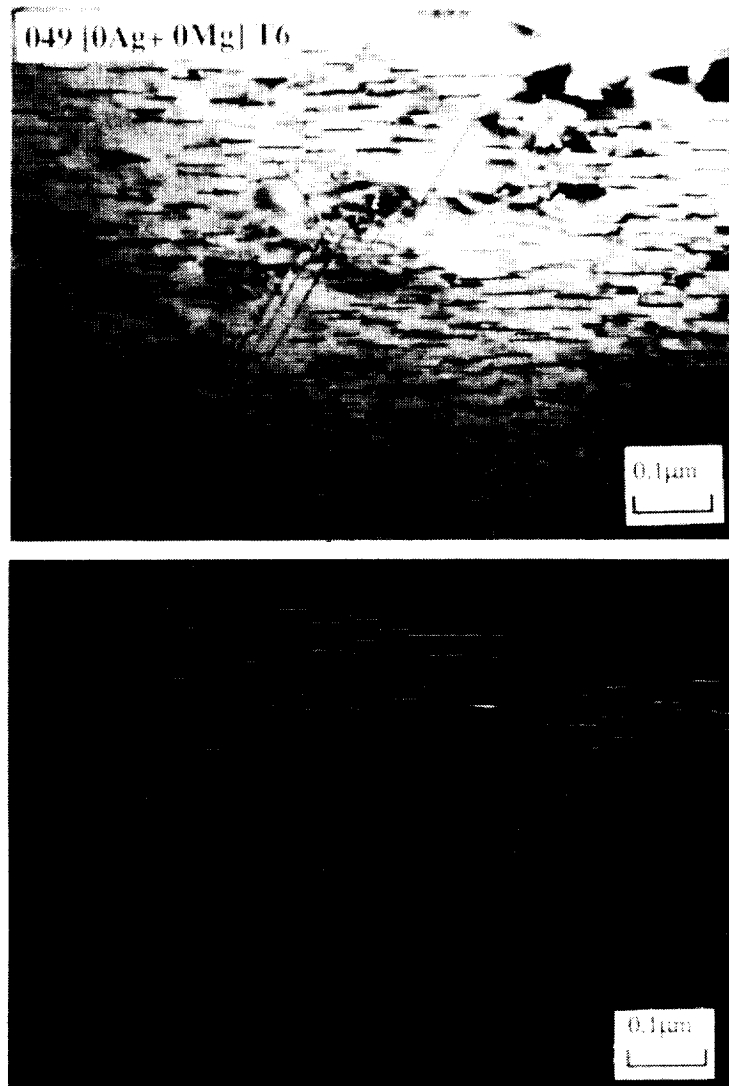FIG. 2   SADPs for alloy 049 T6 with (a) B = [100], (b) B = [110],
and (c) B = [112].

FIG. 3 (a) Brightfield micrograph for 049 [0Ag+0Mg] T6 (B = [110]),
and (b) dark-field micrograph, g = [100].

The BF micrograph for 049 (also imaged with B = [110]) shows a fairly uniform distribution of T_1-type precipitates (Fig.4a) that are about 10Å in thickness and appear to have about the same diameter as the heterogeneous T_1 precipitates in 049[0Ag+0Mg] (Fig. 3a). In this orientation, two T_1 variants are normal to the plane of the foil and two are inclined at about 35° (12). The DF micrograph (Fig. 4b) shows the T_1-type precipitates that are nearly normal to B.

Comparing the T6 microstructures of 049[0Ag+0Mg] and 049 shows that the distribution of the strengthening phases is strongly influenced by the Ag+Mg addition (Table 2).

Table 2
Strengthening Phases After 24 h Aging at 180°C
(based on electron diffraction results)

Alloy	Phases/Diffraction Results	Relative Distribution
049[0Ag+0Mg]	T_1 (Al_2CuLi)	Nonhomogeneous with θ' PFZ
	θ'(Al_2Cu)	Nonhomogeneous; predominant strengthening phase
	α'(Al_3Zr/Al_3Li)	Minor
049	T_1-type; T_1(Al_2CuLi) and/or Ω (Al-Cu)	Homogeneous
	θ'	None
	Al_3Zr	Minor

As shown in Figs. 3b and 5a, a θ' PFZ exists along the GB for 049[0Ag+0Mg]. T_1 precipitates cross the θ' PFZ in 049 [0Ag+0Mg] (Fig. 5 at the arrow) and are present right up to the boundary in 049 (Fig. 5b).

FIG. 4 (a) Brightfield micrograph for 049 T6 (B = [110])
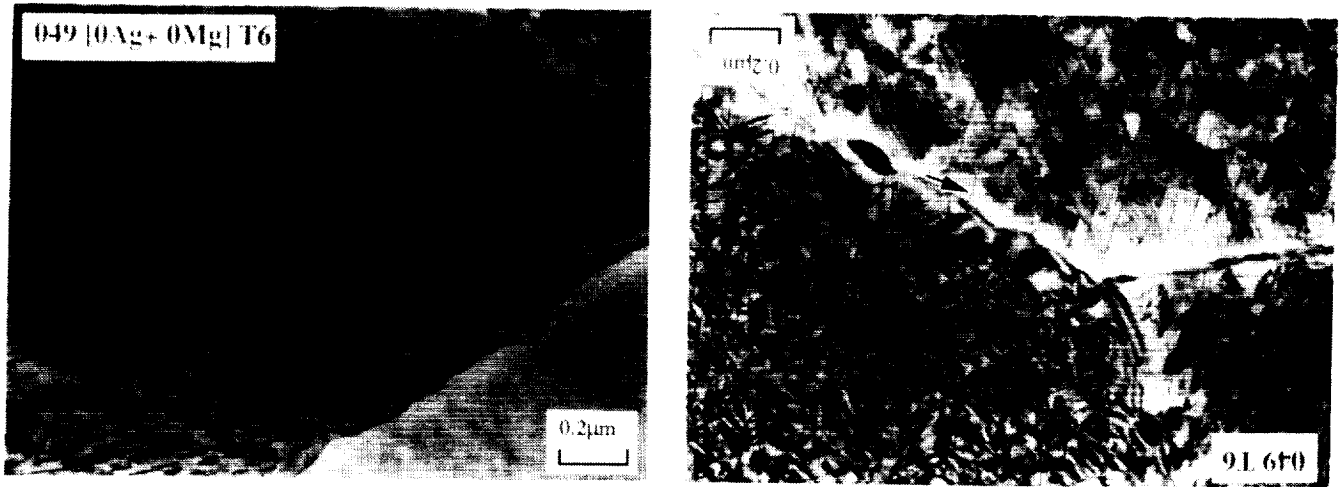and (b) dark-field micrograph using center of <111> streak.

FIG. 5 Brightfield micrographs of high-angle grain boundaries
(B = [110]) in (a) 049[0Ag+0Mg] T6 and (b) 049 T6.

Discussion

The distribution of strengthening phases in the Al-6.3Cu-1.3Li-0.14Zr (wt%) alloy with a Cu/Li wt% ratio of 4.8 is substantially altered by small additions of Ag+Mg. As shown in Fig. 3, θ' and heterogeneous T_1 are the primary strengthening phases in alloy 049[0Ag + 0Mg] artificially aged to a near-peak strength without cold work. Silcock (13) observed the same phase assemblage after artificially aging Al-Cu-Li ternary alloys with similar compositions for 16 h at 165°C. The addition of Ag+Mg (i.e., alloy 049) results in a uniform distribution of fine T_1-type precipitates (Fig. 4). Recent work by Gayle et al. (11) showed that θ', $S'(Al_2CuMg)$, and a phase designated as ν could also be present in the matrix of Weldalite™ 049 in the T6 temper. Although no diffraction was observed from other strengthening precipitates in the present study, it is possible that some may be present at volume fractions that are too low to provide detectable diffraction information on the SADPs. Thus, the Ag+Mg addition results in an increase in the stability of T_1-type precipitates, apparently at the expense of the θ' phase.

Nucleation of T_1 in an Al-2.4Li-2.4Cu-0.18Zr alloy was shown by Cassada et al. (5) to require the presence of Shockley partial dislocations. They (5) proposed that most of the Shockley partials result from cold work after quenching, which is consistent with the finer T_1 distribution and increased strengthening that accompanies increased cold work. In the present study, alloy 049 without prior cold work displays a uniform distribution of fine T_1-type precipitates. Therefore, the addition of Ag+Mg must either significantly

increase the number of Shockley partial dislocations -- unlikely for a non-cold-worked temper -- or enhance the nucleation of T_1-type precipitates by some other mechanism. Perhaps the Ag+Mg increases the number fraction of collapsed vancancy loops (i.e., Frank partial dislocations) which then serve as effective sites for nucleation of T_1-type precipitates.

A number of workers (13-21) have investigated the effect of Ag+Mg on precipitation in Al-Cu alloys. Chester and Polmear (14) identified a novel strengthening phase, which they called Ω. Some controversy exists as to the structure of the Ω-phase, with Kerry and Scott (15) assigning it a hexagonal structure, Auld (19) assigning it a monoclinic structure, and Muddle and Polmear (16) and Knowles and Stobbs (20) assigning it an orthorhombic structure. Auld and Vietz (17) proposed that Ω is isostructural with the T_1-phase (Al_2CuLi) observed in Al-Cu-Li alloys. Regardless of the exact structure of the Ω-phase, Scott et al. (19) showed that when Ag+Mg are added to an Al-Cu alloy, the Ω-phase becomes more stable than 0'; as a result, the volume fraction of the 0'-phase decreases and the volume fraction of the Ω-phase increases with increased artificial aging. Since Mg and Ag additions lower the stacking fault energy (SFE) of aluminum (18), Scott et al. (21) hypothesized that the decreased SFE enhanced segregation of solute to the {111} planes, which then acted as nuclei for the Ω-phase (the Ω-phase has a {111} habit plane in the Al-Cu system).

Faulted loops surrounded by Frank partial dislocations (b=1/3[111]) form when a vacancy disk collapses. As the size of the loop increases, the stacking fault disappears and a complete loop with b = 1/2 [110] is nucleated (22). The critical size at which the complete loop nucleates is

related to the SFE: the lower the SFE, the larger the critical size. The Ag+Mg in alloy 049 could affect the formation and stability of these partials in two ways. First, the high affinity between Mg and vacancies (23) will increase the number of vacancies retained in the microstructure after quenching from the SHT temperature and, consequently, increase the number of vacancies available to form loops. Second, the decrease in SFE induced by Ag+Mg might stabilize the Frank partials (23). Also, the stacking fault could be further stabilized by an increase in the solute concentration on the Frank partial dislocation due to the Suzuki effect (24): solute concentration on the stacking fault is different from that in the matrix due to changes in the chemical potential of the solute. These stacking faults with high solute concentration could then act as nucleation sites for T_1-type precipitates.

In summary, we have shown that the Ag+Mg addition increases the precipitation of T_1-type precipitates on {111} planes in the non-cold worked artificially aged temper and we propose a mechanism whereby an increase in the formation and stability of the Frank partial dislocations provides nuclei for T_1-type precipitates. An investigation is currently under way to determine the Burgers vector of the dislocation at the precipitate-matrix interface.

Acknowledgement

References

1. R.F. Ashton, D.S. Thompson, E.A. Starke, Jr., and F.S. Lin, in Al-Li Alloys III, C. Baker, P.J. Gregson, S.J. Harris, and C.J. Peel, eds., Inst. of Metals, London (1986).

2. T.H. Sanders Jr., and E.A. Starke, Jr., in Proc. of the Fifth Int. Al-Li Conf., T.H. Sanders, Jr., and E.A. Starke, Jr., eds., Mater. and Component Eng. Pub. Ltd., London (1989).

3. T.H. Sanders and E.A. Starke, in Aluminum-Lithium Alloys II, T.H. Sanders, Jr., and E.A. Starke, Jr., eds., TMS-AIME, Warrendale, PA, pp. 1-15 (1983).

4. J.C. Huang and A.J. Ardell, Acta Metall., 36, pp. 2995-3006 (1988).

5. W.A. Cassada, G.J. Shiflet, and E.A. Starke, Jr., in 4th Int. Aluminum-Lithium Conf., G. Champier, B. Dubost, D. Miannay, and L. Sabetay, eds., Soc. Francaise de Metallurgie, Paris, France, pp. C3-397-406 (1987); J. de Physique (France), 1987, 48, (9) (1987).

6. E.W. Lee and W.E. Frazier, Scripta Metall., 22, pp. 53-57 (1988).

7. J.R. Pickens, F.H. Heubaum, T.J. Langan, and L.S. Kramer, ibid. Ref. 2, p. 1397.

8. T.J. Langan and J.R. Pickens, ibid. Ref. 2, p. 691.

9. J.R. Pickens, F.H. Heubaum and L.S. Kramer, Scripta Metall. et Mater., 24, pp. 457-462 (1990).

10. F.W. Gayle, F.H. Heubaum, and J.R. Pickens ibid. ref. 2, pp. 701-710.

11. F.W. Gayle, F.H. Heubaum, and J.R. Pickens, Scripta Metall., 24, pp. 79-84 (1990).

12. A. Kelly and R.B. Nicholson, Prog. Metall. Sci., 10 (3), p. 193 (1963).

13. J.M. Silcock, J. Inst. Metall., 88, pp. 357-364 (1959-60).

14. R.J. Chester and I.J. Polmear, in The Metallurgy of Light Metals, Inst. of Metallurgists, London, pp. 75-81 (1983).

15. S. Kerry and V.D. Scott, Metall. Sci., 18, pp. 289-294 (1984).

16. B.C. Muddle and I.J. Polmear, Acta Metall., 37 (3), pp. 777-789 (1989).

17. J.M. Auld and J.T. Vietz, in The Mechanism of Phase Transformations in Crystalline Solids, 77, The Inst. of Metals, London (1969).

18. P.C.J. Gallagher, Metall. Trans., 1, pp. 2429-2461 (1970).

19. J.H. Auld, Mat. Sci and Tech., 2, pp. 784-787 (1986).

20. K.M. Knowles and W.M. Stobbs, Acta Cryst., B44, pp. 207-227 (1988).

21. V.D. Scott, S. Kerry, and R.L. Trumper, Mater. Sci. and Technol., 3, pp. 827-834 (1987).

22. F. Kroupa, in Theory of Crystal Defects, Proc. of the Summer School held in Hrazany, B. Gruber, ed., Academic Press, NY, pp. 275-316 (1964).

23. K.H. Westmacott, R.S. Barnes, D. Hull, and R.E. Smallman, Philos. Mag., 6, pp. 929-935 (1961).

24. H. Suzuki, Sci. Rep. Res. Inst. Tohoku Univ., A-4, p. 452 (1952).